

Modeling and parameter estimation of rheological objects for simultaneous reproduction of force and deformation

Zhongkui Wang and Shinichi Hirai

Department of Robotics, Ritsumeikan University

Noji-higashi 1-1-1, Kusatsu, 525-8577, Japan

gr046074@ed.ritsumei.ac.jp, hirai@se.ritsumei.ac.jp

Abstract—Many deformable objects in our living life demonstrate rheological behaviors, such as human organs and tissues, clays and various food products. Rheological objects include both elastic and plastic properties. Due to the presence of residual (permanent) deformation, it is difficult to model rheological objects, especially to reproduce both force and residual deformation simultaneously. In this paper, a series of physical models was investigated for simulating rheological behaviors. Generalized formulations of the constitutive laws were derived for serial and parallel physical models, respectively. We found that the serial models are appropriate for formulating strain, whereas the parallel models allow a convenient calculation of stress. Analytical expressions of force and residual deformation were then derived for generalized parallel models. Theoretical discussions suggested the difficulty to reproduce both force and deformation simultaneously using linear physical models. A 2D FE (finite element) model was then formulated and an efficient method for estimating physical parameters were proposed by taking the advantages of analytical force expressions. Experimental results with commercial clay and Japanese sweets material were presented to validate our modeling and parameter estimation methods. A dual-moduli viscous element was also introduced to improve our FE model for reproducing rheological force and deformation simultaneously.

Index Terms—Modeling; Parameter estimation; Rheological object; Finite element method; Simulation.

I. INTRODUCTION

Modeling and simulation of soft deformable objects has been studied for over 20 years [1], [2] and has played an important role in many fields, including computer aided surgery, food automation, and robotics. Deformable objects can be roughly divided into three categories based on their deformation behavior: elastic object, in which the deformation is completely reversible; plastic object, in which the deformation is completely maintained; and rheological object, in which the deformation is partly reversible. Previous work on modeling of deformable objects has mainly focused on elastic and visco-elastic objects, especially in surgical applications since most biological organs and tissues seem to be recoverable after loading-unloading operations. Some organs and tissues, however, may fail to completely recover from the deformation. Hrapko *et al.* found that porcine brain tissue did not recover completely after a loading-unloading cycle [3]. In vivo experimental results showed that residual deformation may also present in human liver [4]. In addition, many other deformable objects, such as clay and various food products, demonstrate rheological behaviors. Chua *et al.* stated that the most critical barrier against the

application of robotics and automation in food industry is a lack of understanding of the food product properties as an “engineering” material for handling operations [5]. To date, modeling of 2D/3D rheological objects have not been well developed and an effective method for determining physical properties of rheological object as an “engineering” material has not yet been established.

Generally, modeling a rheological object is more difficult than modeling an elastic or plastic object due to the presence of residual deformation. Early work on the modeling of rheological objects dates back to Terzopoulos *et al.* [2], who have proposed several physical models to describe inelastic objects and a Burgers model was introduced to describe rheological behaviors. However, it is only a conceptual description and they did not give any simulation results and information of parameter determination. A particle-based (or mass-spring-damper) model was employed to model a food dough and a method for calibrating its physical parameters was proposed based on a genetic algorithm (GA) optimization [6], [7]. The particle-based model has an advantage of less computation costs [8], but the formulation was not based on continuum mechanics and the simulation accuracy is quite limited. A two-layered Maxwell model [9] and Fung’s viscoelastic model [10] has been used respectively to reproduce the force response of a “Norimaki-sushi” when grasped by a robot hand. Good approximations of force behaviors were obtained. Unfortunately, both models are 1D cases. In addition, the ISU exoskeleton technique has been used in modeling clay to simulate an interaction between virtual clay and a human finger [11].

Interestingly, above-mentioned work has focused on either reproduction of deformation alone [6], [7] or reproduction of force alone [9], [10]. None of them considered both. However, in some application, *e.g.*, surgical simulation with haptic feedback or virtual manipulation of food products, accurate results of both force and deformation are necessary. Both force and deformation behaviors of organs and tissues were considered simultaneously in an *ex vivo* and an *in vivo* property characterization of porcine livers [12], [13]. However to our knowledge, in current surgical related applications, organs and tissues were mostly supposed to be elastic or visco-elastic and no residual deformation was taken into consideration.

In our previous work, we have developed FE models for simulating various deformable objects [14]. A three-

element [15] and a four-element [16] models were employed respectively to describe rheological behaviors. A method for identifying physical parameters was proposed based on iterative optimization [16]. We found that the four-element model was more appropriate than the three-element model for reproducing rheological forces. In addition, experimental results with commercial clay indicated that a contradiction between the reproductions of force and residual deformation may exist due to the linearity of the physical model.

In this paper, we summarized the physical models which could be used to represent rheological behaviors. According to the configuration among elements, we divided the physical models into two groups: serial and parallel models. A general constitutive law for each configuration was formulated. To analyze the reason of the contradiction between reproductions of force and residual deformation, analytical expressions of force and residual deformation were derived and discussions were done. Two-dimensional FE dynamic model was then given with simpler formulation comparing with the previous one. Based on the analytical expressions of rheological forces, a more efficient method for estimating the physical parameters was proposed. Experimental results with commercial clay and Japanese sweets material were presented to validate our discussions and methods. Finally, a dual-moduli viscous element was introduced to improve our current model for simultaneously reproducing both rheological force and deformation.

II. SUMMARIZATION OF PHYSICAL MODELS

Physical models are often employed to describe deformable materials and objects, *e.g.*, an elastic element (Fig. 1a) and a viscous element (Fig. 1b) represent ideal elastic and viscous material, respectively. An elastic and a viscous elements connected in series was called a Maxwell element (Fig. 1c), which denotes a simplest rheological material. An elastic and a viscous elements connected in parallel was called a Kelvin (sometimes called Kelvin-Voigt) element (Fig. 1d), which denotes a visco-elastic material. We refer the above four elements as basic elements. By connecting some basic elements in different configurations, many physical models could be obtained for simulating rheological behaviors. We divided such models into two groups: serial and parallel models (Fig. 2).

A. Generalized Serial Model

A serial rheological model consists of numbers of Kelvin elements and a viscous or a Maxwell element connected in

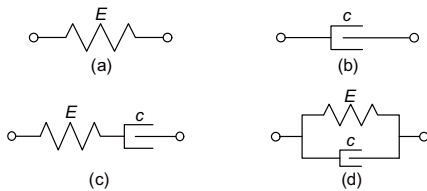


Fig. 1. The basic elements for describing deformable materials: (a) the elastic; (b) the viscous; (c) the Maxwell; and (d) the Kelvin elements.

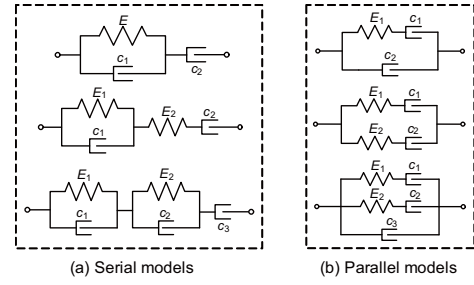


Fig. 2. 2 groups of rheological models: (a) serial, and (b) parallel models.

series. Note that the deformation generated in an elastic or a Kelvin element is completely recoverable. Therefore, a serial rheological model must include a viscous element connected in series, which causes the residual (permanent) deformation. According to the presence of elastic element, serial models can be divided into two types, as shown in Fig. 3. Let us take the type 1 model as an example to show the derivation procedure of the constitutive law.

Note that the constitutive law of four basic elements were formulated as:

$$\begin{aligned}
 \text{Elastic element : } & \sigma = E\varepsilon, \\
 \text{Viscous element : } & \sigma = c\dot{\varepsilon}, \\
 \text{Maxwell element : } & \dot{\sigma} + \frac{E}{c}\sigma = E\dot{\varepsilon}, \\
 \text{Kelvin element : } & \sigma = E\varepsilon + c\dot{\varepsilon},
 \end{aligned} \tag{1}$$

where vector $\bar{\sigma}$ and $\bar{\varepsilon}$ are the stress and strain generated in basic elements. Constants E and c are the Young's modulus and viscous modulus of elastic and viscous elements, respectively.

Let ε_i and ε_{n+1} be the strain at the i -th Kelvin element and the $(n+1)$ -th viscous element, respectively. Let E_i and c_i be the Young's modulus and viscous modulus of the i -th elastic and viscous elements, respectively. Due to the serial connections among these basic elements, the total stress at the serial model is equal to the stress at each basic element and the total strain at the serial model is equal to the sum of the strains at all basic elements. That is,

$$\begin{aligned}
 \sigma &= E_i\varepsilon_i + c_i\dot{\varepsilon}_i, \quad 1 \leq i \leq n, \\
 \sigma &= c_{n+1}\dot{\varepsilon}_{n+1}, \\
 \varepsilon &= \sum_{i=1}^{n+1} \varepsilon_i.
 \end{aligned} \tag{2}$$

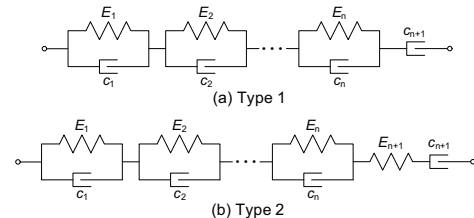


Fig. 3. Generalized serial models: (a) type 1; and (b) type 2.

Taking Laplace transform of the above equations, we have

$$\begin{aligned}\sigma(s) &= E_i \varepsilon_i(s) + c_i s \varepsilon_i(s), \quad 1 \leq i \leq n, \\ \sigma(s) &= c_{n+1} s \varepsilon_{n+1}(s), \\ \varepsilon(s) &= \sum_{i=1}^{n+1} \varepsilon_i(s).\end{aligned}\quad (3)$$

Eliminating $\varepsilon_i(s)$ from the above equations, we then have

$$\varepsilon(s) = \left[\left(\sum_{i=1}^n \frac{1}{s+r_i} \frac{1}{c_i} \right) + \left(\frac{1}{s} \frac{1}{c_{n+1}} \right) \right] \sigma(s), \quad (4)$$

where $r_i = E_i/c_i$. Let us define a polynomial as below:

$$\prod_{i=1}^n (s+r_i) = A_n s^n + A_{n-1} s^{n-1} + \cdots + A_1 s + A_0. \quad (5)$$

The coefficients of the above polynomial have the forms of:

$$A_n = 1, \quad A_{n-1} = \sum_{i=1}^n r_i, \quad A_{n-2} = \sum_{i=1}^n \sum_{\substack{j=1 \\ j \neq i}}^n r_i r_j, \quad \cdots, \quad A_0 = \prod_{i=1}^n r_i. \quad (6)$$

Multiplying Eq. 4 by Eq. 5, we have

$$\begin{aligned}\prod_{i=1}^n (s+r_i) \varepsilon(s) &= \prod_{i=1}^n (s+r_i) \left[\left(\sum_{i=1}^n \frac{1}{s+r_i} \frac{1}{c_i} \right) + \left(\frac{1}{s} \frac{1}{c_{n+1}} \right) \right] \sigma(s) \\ &= \left[\sum_{i=1}^n \prod_{\substack{j=1 \\ j \neq i}}^n \frac{(s+r_j)}{c_i} + \prod_{j=1}^n \frac{s+r_j}{s} \frac{1}{c_{n+1}} \right] \sigma(s).\end{aligned}\quad (7)$$

We then find the following equation:

$$\begin{aligned}\prod_{\substack{j=1 \\ j \neq i}}^n (s+r_j) &= (s+r_1) \cdots (s+r_{i-1})(s+r_{i+1}) \cdots (s+r_n) \\ &= s^{n-1} + B_{i,1} s^{n-2} + \cdots + B_{i,n-2} s + B_{i,n-1},\end{aligned}\quad (8)$$

where

$$B_{i,1} = \sum_{\substack{j=1 \\ j \neq i}}^n r_j, \quad B_{i,2} = \sum_{\substack{j=1 \\ j \neq i}}^n \sum_{\substack{k=1 \\ k \neq i}}^n r_j r_k, \quad \cdots, \quad B_{i,n-1} = \prod_{\substack{j=1 \\ j \neq i}}^n r_j. \quad (9)$$

Substituting Eqs. 5 and 8 into Eq. 7, we have the following Laplace transform equation:

$$\begin{aligned}(A_n s^{n+1} + A_{n-1} s^n + \cdots + A_0 s) \varepsilon(s) \\ = (B_n^{s1} s^n + B_{n-1}^{s1} s^{n-1} + \cdots + B_1^{s1} s + B_0^{s1}) \sigma(s),\end{aligned}\quad (10)$$

where

$$B_n^{s1} = \sum_{i=1}^n \frac{1}{c_i} + \frac{A_n}{c_{n+1}}, \quad B_{n-1}^{s1} = \sum_{i=1}^n \frac{B_{i,1}}{c_i} + \frac{A_{n-1}}{c_{n+1}}, \quad \cdots, \quad B_0^{s1} = \frac{A_0}{c_{n+1}}. \quad (11)$$

Applying the inverse Laplace transform to Eq. 10 yields the constitutive law of serial model of type 1 as follows:

$$\sum_{i=1}^{n+1} A_{i-1} \frac{\partial^i \varepsilon}{\partial t^i} = \sum_{j=0}^n B_j^{s1} \frac{\partial^j \sigma}{\partial t^j}. \quad (12)$$

Note that the highest-order derivative of strain ε is one order larger than the highest-order of stress σ . In addition, there

is no constant term in the coefficients of strain polynomial (the left side of Eq. 12).

Following the same derivation procedure, we could obtain the constitutive law of serial model of type 2 as follows:

$$\sum_{i=1}^{n+1} A_{i-1} \frac{\partial^i \varepsilon}{\partial t^i} = \sum_{j=0}^{n+1} B_j^{s2} \frac{\partial^j \sigma}{\partial t^j}, \quad (13)$$

where

$$B_{n+1}^{s2} = \frac{1}{E_{n+1}}, \quad B_n^{s2} = \sum_{i=1}^n \frac{1}{c_i} + \frac{A_n}{c_{n+1}} + \frac{A_{n-1}}{E_{n+1}}, \quad \cdots, \quad B_0^{s2} = \frac{A_0}{c_{n+1}}. \quad (14)$$

Equation 13 suggested that the highest-order derivative of strain ε is equal to the highest-order of stress σ . Note that the left side of Eq. 13 has the same form with the left side of Eq. 12.

B. Generalized Parallel Models

Two kinds of parallel rheological models were shown in Fig. 4. Due to the parallel connections among basic elements, the total strain at the parallel model is equal to the strain at each basic element and the total stress at the parallel model is equal to the sum of the stress at all basic elements. For parallel model of type 1, we therefore have

$$\begin{aligned}\dot{\sigma}_i + \frac{E_i}{c_i} \sigma_i &= E_i \dot{\varepsilon}, \quad 1 \leq i \leq n, \\ \sigma_{n+1} &= c_{n+1} \dot{\varepsilon}, \\ \sigma &= \sum_{i=1}^{n+1} \sigma_i.\end{aligned}\quad (15)$$

Following the same derivation with serial models, we could end up with the constitutive law of parallel model of type 1 (Fig. 4a) as follows:

$$\sum_{i=0}^n A_i \frac{\partial^i \sigma}{\partial t^i} = \sum_{j=1}^{n+1} B_j^{p1} \frac{\partial^j \varepsilon}{\partial t^j}, \quad (16)$$

where

$$\begin{aligned}B_{n+1}^{p1} &= c_{n+1}, \quad B_n^{p1} = \sum_{i=1}^n E_i + A_{n-1} c_{n+1}, \\ \cdots, \quad B_1^{p1} &= \sum_{i=1}^n B_{i,n-1} E_i + A_0 c_{n+1}.\end{aligned}\quad (17)$$

Correspondingly, the constitutive law of parallel model of type 2 (Fig. 4b) could be formulated as:

$$\sum_{i=0}^n A_i \frac{\partial^i \sigma}{\partial t^i} = \sum_{j=1}^n B_j^{p2} \frac{\partial^j \varepsilon}{\partial t^j}, \quad (18)$$

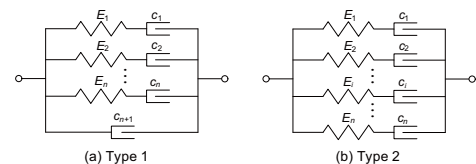


Fig. 4. Generalized parallel models: (a) type 1; and (b) type 2.

where

$$B_n^{p2} = \sum_{i=1}^n E_i, B_{n-1}^{p2} = \sum_{i=1}^n B_{i,1} E_i, \dots, B_1^{p2} = \sum_{i=1}^n B_{i,n-1} E_i. \quad (19)$$

According to Eqs. 12, 13, 16, and 18, we found that the constitutive law of serial model of type 1 (Eq. 12) has the identical form with the parallel model of type 1 (Eq. 16) except some coefficients having different formulations. Correspondingly, the constitutive laws of serial model of type 2 (Eq. 13) also has the same form with the parallel model of type 2 (Eq. 18) by replacing the summation limit $n+1$ in Eq. 13 by n . Note that same constitutive laws yield same deformation behaviors. Therefore, for simulating a certain behavior, we could use either a serial model or a parallel model. Actually, for any type of physical model, which consists of any numbers of basic elements connected in any configuration, we are always able to find a corresponding serial or parallel model which yields the same behaviors. This allows us to investigate only one representative model instead of analyzing all models for understanding the ability of physical models. In this paper, we investigated the parallel models. In addition, according to Eq. 2, if the total stress at the serial model was available, we could easily calculate the total strain by summing up the individual strain at each element due to the independence among these strains. On the other hand, Eq. 15 indicated that the convenient calculation of rheological force could be achieved by using the parallel models.

III. ANALYSIS OF PARALLEL MODEL

A. Experimental Rheological Behaviors

Typical rheological behaviors (force and deformed shapes) of commercial available clay and Japanese sweets material were shown in Fig. 5. The sweets materials were provided by OIMATU, a sweets company in Kyoto. Two flat squared objects made of the above-mentioned two materials were pushed respectively by a motorized stage with a constant velocity during the pushing phase ($0 \leq t \leq t_p$). Before unloading, the deformed shapes were maintained for a while, which was called holding phase ($t_p \leq t \leq t_p + t_h$). The rheological forces (Fig. 5a-1 and 5b-1) were measured by a tactile sensor and deformed shapes (initial, held, and final shapes as shown Fig. 5a-2 and 5b-2) were recorded by a calibrated camera. During the pushing phase, the rheological forces were increasing with the deformation increasing. During the holding phase, however, the deformed shapes were kept unchanged while the rheological forces were decreasing (force relaxation). After unloading, the rheological forces went to zero and the deformed shapes were partially recovered. Figure 5 showed that rheological behaviors of different materials are quite different. Comparing with clay, the force relaxation behavior of sweets material was slower and the recovered deformation was smaller. Our target is to find an appropriate model to reproduce both rheological force and deformation behaviors simultaneously. Let us now investigate the ability of generalized parallel model for achieving this target.

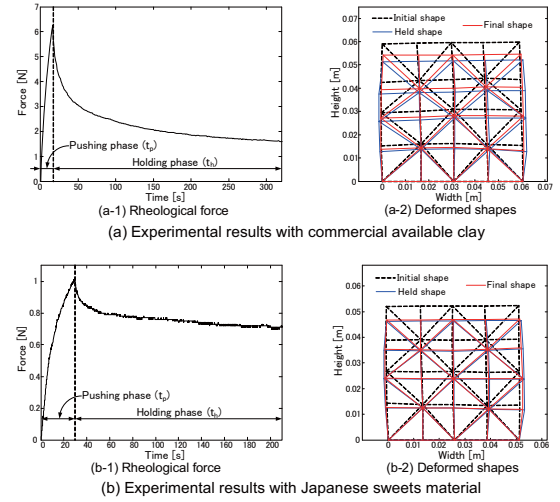


Fig. 5. Typical rheological behaviors of: (a) commercial available clay, and (b) Japanese sweets material.

B. Analytical Expression of Rheological Force

We took the parallel model of type 1 as an example to show the derivation. In the pushing phase, we suppose the strain rate is constant, *i.e.*, $\dot{\epsilon} = p$. Solving Eq. 15, we have the analytical force expression in the pushing phase as below:

$$\sigma(t) = \sum_{i=1}^n c_i p (1 - e^{-\frac{E_i}{c_i} t}) + c_{n+1} p, \quad (0 \leq t \leq t_p). \quad (20)$$

In the holding phase, solving Eq. (15) with $\dot{\epsilon} = 0$ and initial condition of $\sigma_i(t_p)$, we can formulate the analytical force expression in this phase as:

$$\sigma(t) = \sum_{i=1}^n c_i p (1 - e^{-\frac{E_i}{c_i} t_p}) e^{-\frac{E_i}{c_i} (t - t_p)}, \quad (t_p \leq t \leq t_p + t_h). \quad (21)$$

C. Analytical Expression of Residual Deformation

After unloading, we intuitively considered to solve the constitutive law Eq. 16 with $\sigma = 0$ to formulate the strain recovering curve. However, when the order of time derivative of strain ϵ exceeds two, it becomes impossible to solve Eq. 16 because we have no information about the initial condition of strain derivative. We therefore turn our focusing to each viscous element which dominates the residual strain. Let $\epsilon_i^{ela}(t)$ and $\epsilon_i^{vis}(t)$ be the strain at each elastic and viscous element, respectively. Note that the stress at a Maxwell element is equal to the stress at the elastic element and the viscous element as well. Thus, total stress after unloading could be formulated as:

$$\sigma(t) = \sum_{i=1}^{n+1} \sigma_i(t) = \sum_{i=1}^n c_i \dot{\epsilon}_i^{vis}(t) + c_{n+1} \dot{\epsilon}(t) = 0. \quad (22)$$

Integrating the above equation from time $t_p + t_h$ to time infinity, we have

$$\sum_{i=1}^n c_i \int_{t_p + t_h}^{\infty} \dot{\epsilon}_i^{vis}(t) dt + c_{n+1} \int_{t_p + t_h}^{\infty} \dot{\epsilon}(t) dt = 0, \quad (23)$$

and thus

$$\sum_{i=1}^n c_i [\varepsilon_i^{\text{vis}}(\infty) - \varepsilon_i^{\text{vis}}(t_p + t_h)] + c_{n+1} [\varepsilon(\infty) - \varepsilon(t_p + t_h)] = 0. \quad (24)$$

It is important to note that the residual strain at every viscous element in a parallel model should be the same and equal to the total residual strain when time goes to infinity, *i.e.*, $\varepsilon_1^{\text{vis}}(\infty) = \varepsilon_2^{\text{vis}}(\infty) = \dots = \varepsilon_n^{\text{vis}}(\infty) = \varepsilon(\infty)$, because all elastic elements completely recovered from the deformation. Thus, Eq. 24 yields

$$\varepsilon(\infty) = \sum_{i=1}^n \frac{c_i \varepsilon_i^{\text{vis}}(t_p + t_h)}{\sum_{j=1}^{n+1} c_j} + \frac{c_{n+1} \varepsilon(t_p + t_h)}{\sum_{j=1}^{n+1} c_j}. \quad (25)$$

Each viscous element has its own constitutive law as $\sigma_i = c_i \dot{\varepsilon}_i^{\text{vis}}$. Integrating this law through time 0 to time $t_p + t_h$, we have

$$\varepsilon_i^{\text{vis}}(t_p + t_h) = \frac{1}{c_i} \int_0^{t_p + t_h} \sigma_i(t) dt. \quad (26)$$

Substituting Eq. 26 into Eq. 25 and considering $\sigma(t) = \sum_{i=1}^{n+1} \sigma_i(t)$, we finally end up with the expression of total residual strain:

$$\varepsilon(\infty) = \frac{1}{\sum_{i=1}^{n+1} c_i} \int_0^{t_p + t_h} \sigma(t) dt. \quad (27)$$

This equation indicates that the final residual deformation of a parallel rheological model depended on the sum of viscous moduli and the integration of force through the pushing and holding phase.

For the parallel model of type 2, we could obtain the same formulations of force expression in the holding phase and the same formulation of final residual deformation with the summation limit $n + 1$ replaced by n in Eq. 27. The only difference of the parallel model of type 2 is the force expression in the pushing phase, which is given by

$$\sigma(t) = \sum_{i=1}^n c_i p (1 - e^{-\frac{E_i}{c_i} t}), \quad (0 \leq t \leq t_p). \quad (28)$$

D. Discussions

Typical simulation results of rheological stress and strain were shown in Fig. 6 by using a 5-element model (the last row of Fig. 2b) and a 2-layered Maxwell model (the middle row of Fig. 2b). According to Eqs. 20, 21, and 28, we found that the stress curve was determined by viscous moduli c_i and time coefficients E_i/c_i of exponential functions. The coefficients E_i/c_i determine the changing tendency in stress during the holding phase, as formulated in Eq. 21. In order to obtain similar force relaxation curve as shown in Fig. 5, at least two exponential terms are needed, one with large value of E_i/c_i and another one with small E_i/c_i . The large E_i/c_i describes the rapid decreasing in force and the small one denotes the slow decreasing. For example, the stress curves in Fig. 6 were both simulated with coefficients of $E_1/c_1 = 0.005$ and $E_2/c_2 = 0.5$. After determining coefficients E_i/c_i , Eq. 20 could be used to determine the viscous moduli c_i , which dominated stress amplitude $\sigma(t)$ in the pushing phase. Note that there is a sudden drop in stress (Fig. 6a) at the end of

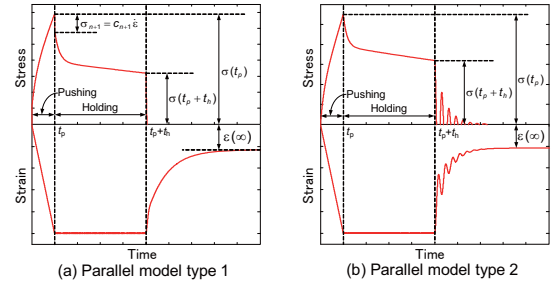


Fig. 6. Typical simulation results of rheological behaviors by using: (a) 5-element model, and (b) 2-layered Maxwell model.

pushing phase for 5-element model (parallel type 1). This sudden drop was denoted by $\sigma = c_{n+1} \dot{\varepsilon}$. Figure 6b showed that the 2-layered Maxwell model (parallel type 2) results in attenuated vibrations in both stress and strain after unloading (Fig. 6b). Based on the above discussion, we could say that the parallel model has the ability of reproducing rheological force behaviors. Our previous work [16] has shown good reproduction of rheological force for commercial clay. However, we failed to reproduce the recovered shape.

Equation 27 implies that the residual strain is dominated by the sum of viscous moduli c_i . On the other hand, parameters c_i also strongly affect force amplitude as formulated in Eqs. 20, 21, and 28. This caused a contradiction between the reproduction of rheological force and recovered shape. For example, if we determine the parameters c_i from force data, the sum of c_i will therefore yields a certain recovered shape. We are unable to change this shape to our desired one. On the contrary, if we firstly calculated the sum of c_i based on Eq. 27, we have an upper limit ($\sum_{i=1}^{n+1} c_i$) for each modulus c_i and we have to keep each c_i under this limit during the reproduction of force behaviors. For some materials, we may be able to achieve a good reproduction of force with c_i under the limit. For most materials, however, this limit was always broken in order to well capture the force curve. The above discussion suggests that parallel model do not have the ability to reproduce both rheological force and deformation simultaneously. Section 5 will give quantitative discussion of this problem. The discussion in Section 2 indicated that we could always find a corresponding parallel model for arbitrary physical model. We can therefore conclude that physical models are not able to reproduce both rheological force and deformation simultaneously for most rheological objects.

IV. FE DYNAMIC MODEL AND PARAMETER ESTIMATION

A. Formulation of FE Dynamic Model

The FE method has proven to be a powerful tool for simulating complex behaviors of deformable objects. In FE simulation, an object is described by a set of elements (*e.g.*, triangles in 2D and tetrahedrons in 3D). The dynamic behaviors of the object are then determined by analyzing the behaviors of individual elements. In this paper, we employ a 2-layered Maxwell model as an example to present 2D FE dynamic model. We constructed a 2D object with triangle

mesh (Fig. 5a-2 and 5b-2) and attached the two-layered Maxwell model onto each triangle. Let vectors \mathbf{u}_N and \mathbf{v}_N be a set of displacements and velocities of nodal points in 2D mesh. Let vectors \mathbf{F}_{2D}^{rheo} and \mathbf{F}^{ext} be a set of rheological forces and external forces on nodal points. Following the same formulation procedure presented in our previous work [14], [15], [16], we could end up with an FE dynamic model consists of following differential equations:

$$\begin{aligned} \dot{\mathbf{u}}_N &= \mathbf{v}_N, \\ \mathbf{M}\dot{\mathbf{v}}_N - \mathbf{A}\boldsymbol{\lambda} &= -\mathbf{F}_{2D}^{rheo} + \mathbf{F}^{ext}, \\ -\mathbf{A}^T\dot{\mathbf{v}}_N &= \mathbf{A}^T(2\omega\mathbf{v}_N + \omega^2\mathbf{u}_N), \\ \dot{\mathbf{F}}_1 &= -\frac{E_1}{c_1}\mathbf{F}_1 + (\lambda_1^{ela}\mathbf{J}_\lambda + \mu_1^{ela}\mathbf{J}_\mu)\mathbf{v}_N, \\ \dot{\mathbf{F}}_2 &= -\frac{E_2}{c_2}\mathbf{F}_2 + (\lambda_2^{ela}\mathbf{J}_\lambda + \mu_2^{ela}\mathbf{J}_\mu)\mathbf{v}_N, \end{aligned} \quad (29)$$

where the last two equations were obtained from the first equation of Eq. 15 by changing 1D stress-strain relationship to 2D force-displacement relationship. Two-dimensional rheological force could be therefore formulated as

$$\mathbf{F}_{2D}^{rheo} = \mathbf{F}_1 + \mathbf{F}_2. \quad (30)$$

Let γ be the Poisson's ratio and then variables λ_1^{ela} , μ_1^{ela} , λ_2^{ela} , and μ_2^{ela} could be calculated as follows:

$$\lambda_i^{ela} = \frac{E_i\gamma}{(1+\gamma)(1-2\gamma)}, \quad \mu_i^{ela} = \frac{E_i}{2(1+\gamma)}, \quad (i=1,2).$$

The detailed definition and description of other variables and matrixes can be found in our previous work [14], [15], [16].

Comparing with our previous FE dynamic model, this model has a simpler formulation. This should thank to the advantage of parallel physical model, in which each layer of Maxwell element has an independent stress. Using Eq. 29, we can simulate rheological behaviors and typical results were shown in Fig. 6b.

B. Parameter Estimation

Before simulating any real objects, their physical parameters have to be available in advance. In the above FE model, there are a total of 5 unknown parameters: E_1 , E_2 , c_1 , c_2 , and γ . Our previous work [16] has proposed an approach to identify these parameters based on iterative FE simulation and nonlinear optimization. The idea is to iterate FE simulation with updated physical parameters until the difference between simulation and experiment becomes minimal. In [16], we found that we could estimate the Poisson's ratio γ separately because only γ affected the held shape. We could then identify other parameters by minimizing force difference. This method is simple and works well but it is time-consuming. For force optimization, it took hours or days (depends on initial parameter setting) to obtain results. However, according to the analysis in the previous section, we can take the advantage of analytical force expression to develop a more efficient method.

Extending Eqs. 28 and 21 to 2D formulations, we have

$$\mathbf{F}(t) = \sum_{i=1}^n c_i (1 - e^{-\frac{E_i}{c_i}t}) \mathbf{M}_\gamma \mathbf{v}_N^{Push}, \quad (0 \leq t \leq t_p), \quad (31)$$

$$\mathbf{F}(t) = \sum_{i=1}^n c_i (1 - e^{-\frac{E_i}{c_i}t_p}) e^{-\frac{E_i}{c_i}(t-t_p)} \mathbf{M}_\gamma \mathbf{v}_N^{Push}, \quad (t_p \leq t \leq t_p + t_h), \quad (32)$$

where

$$\mathbf{M}_\gamma = \gamma \lambda \mathbf{J}_\lambda + \gamma \mu \mathbf{J}_\mu = \frac{\gamma}{(1+\gamma)(1-2\gamma)} \mathbf{J}_\lambda + \frac{1}{2(1+\gamma)} \mathbf{J}_\mu.$$

Vector \mathbf{v}_N^{Push} could be obtained from the simulation results in the pushing phase with the known Poisson's ratio γ .

An objective function is defined to be:

$$e(\theta) = \sum_{i=1}^N \|\mathbf{f}_i^{exp} - \mathbf{f}_i^{cal}(t, \theta)\|^2, \quad (33)$$

where N is the number of sampling points, vector \mathbf{f}_i^{exp} and $\mathbf{f}_i^{cal}(t, \theta)$ are experimental forces and calculated forces, respectively, at the i -th sampling time, and vector θ is the parameters to be estimated. The optimization is terminated when the tolerance on $e(\theta)$ or the tolerance on θ less than a threshold, 1×10^{-6} . The basic estimation algorithm is as follows:

- 1) Initial setting of material parameters.
- 2) Using Eqs. 31 and 32 to calculate force.
- 3) Using Eq. 33 to calculate the objective function.
- 4) If the terminate conditions are not satisfied, adjust parameters and repeat steps 2–3.

This method is much faster than our previous simulation-based method. We could obtain a solution with only several seconds by using MATLAB optimization toolbox.

In addition, extending Eq. 27 to 2D formulation, we have

$$\mathbf{M}_\gamma \mathbf{u}_N(\infty) = \frac{1}{\sum_{i=1}^{n+1} c_i} \int_0^{t_p+t_h} \mathbf{F}(t) dt. \quad (34)$$

Note that residual deformation $\mathbf{u}_N(\infty)$ and force data $\mathbf{F}(t)$ are available from experimental measurements. Matrix \mathbf{M}_γ can be prepared in advance since it only depends on initial geometrical coordinates and Poisson's ratio γ . This equation allows us to calculate the sum of viscous moduli $\sum_{i=1}^{n+1} c_i$.

V. VALIDATION AND NONLINEAR MODEL

A. Experimental Validation

Experimental data shown in Fig. 5 were taken as examples to quantitatively demonstrate the contradiction in reproduction of rheological force and residual deformation. We employed the two-layered Maxwell model and Eq. 29 to simulate the behaviors of these two objects. Using the parameter estimation methods proposed in the last section, we obtained two sets of physical parameters for each material, as given in Table I. The first set of parameters was estimated by minimizing the force difference without considering the final residual deformation. In other words, we used four unknown parameters (E_1 , E_2 , c_1 , and c_2) to optimize Eq. 33. During the estimation of the second set of parameters, however, we took the residual deformation into consideration by using Eq. 34 to calculate $c_1 + c_2$, as given in the second column of Table I. The other three parameters were then estimated by minimizing force difference. Table I suggested that large values of $c_1 + c_2$ were needed to achieve good

TABLE I
ESTIMATED PARAMETERS FOR BOTH MATERIALS

Material	$c_1 + c_2$ (Pa·s)	γ	E_1 (Pa)	E_2 (Pa)	c_1 (Pa·s)	c_2 (Pa·s)	$e(\theta)$ (N ²)
Clay	1.3988×10^7	0.2902	3.1753×10^4	7.2168×10^4	1.3291×10^7	6.9737×10^5	4.0794
	9.6961×10^6		3.7731×10^4	8.0952×10^4	9.2023×10^6	4.9380×10^5	24.515
Sweets	1.3328×10^7	0.3353	1.0553×10^4	3.7340×10^4	1.3212×10^7	1.1602×10^5	0.8388
	1.6849×10^6		2.8909×10^3	1.1612×10^4	3.3585×10^5	1.3491×10^6	186.48

reproduction of rheological forces for both materials, where clay has $c_1 + c_2 = 1.3988 \times 10^7$ Pa·s and sweets material has $c_1 + c_2 = 1.3328 \times 10^7$ Pa·s. However, in order to well reproduce the final recovered shape, small values of $c_1 + c_2$ are necessary, e.g., $c_1 + c_2 = 9.6961 \times 10^6$ Pa·s for clay and $c_1 + c_2 = 1.6849 \times 10^6$ Pa·s for sweets material. For both materials, the values of $c_1 + c_2$ for force reproduction are larger than the values for deformation reproduction. We failed to satisfy the requirement of value $c_1 + c_2$ for both force and deformation reproduction. Two values of $c_1 + c_2$ for clay are quite close but very different for sweets material. It indicated that it is more difficult for sweets material to reproduce force and deformation behaviors simultaneously.

Using the estimated parameters listed in Table I, we could simulate the rheological behaviors of both materials. Comparison between simulation results and experimental measurements were shown in Figs. 7 and 8, where Figs. 7a and 8a were simulated with the first set of parameters (Table I) for both materials and Figs. 7b and 8b were with the second set of parameters. We found that clay has more coincident results than sweets material using two sets of parameters. This again attributes to the value of $c_1 + c_2$ with close values of $c_1 + c_2$ resulting in more coincident results, and vice versa. Figure 8 suggested that it is impossible for sweets material to reproduce both force and deformation behaviors simultaneously by using the two-layered Maxwell model. This impossibility will not be changed by adding more elements on the physical model or by changing the configuration among basic elements. This impossibility comes from the linearity of the basic elements, especially the linear viscous element which dominates both stress amplitude and

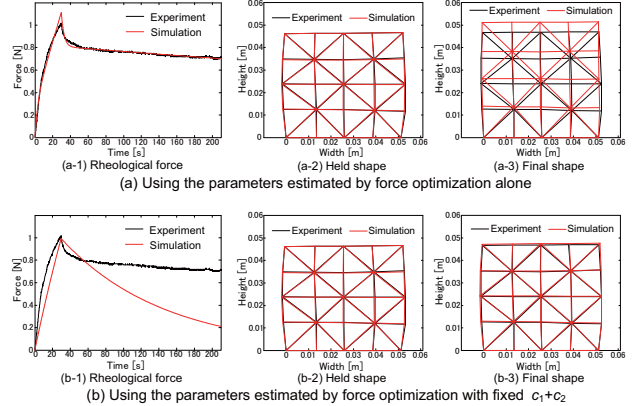


Fig. 8. Validation results of Japanese sweets material.

residual strain. Figures 7 and 8 also showed that the held shapes simulated with different sets of parameters have the identical results and quite close to the experimental measurements. This is because the held shape was only affected by the Poisson's ratio γ [16] and our FE model can reproduce both force and held shape simultaneously. In addition, it is necessary to mention that the Poisson's ratios γ listed in Table I were estimated in advance by minimizing the difference of the held shape between simulation and experiment.

B. Introduction of Dual-Moduli Viscous Element

According to the above discussions, we found that the parameter $c_1 + c_2$ must take different values through the simulation to capture both force and residual deformation. We therefore formulated a viscous element as

$$\sigma(t) = (\kappa\alpha + c)\dot{\epsilon}(t), \quad (35)$$

where scalars α and c were parameters to be determined. Switch function κ takes the following value:

$$\kappa = \begin{cases} 1 & t \leq t_p + t_h; \\ -1 & t > t_p + t_h. \end{cases} \quad (36)$$

This dual-moduli viscous element has an ability to switch the parameters from one set to another during simulation. Introducing Eq. 35 into our FE model, we could modify our FE model by replacing the last two differential equations of

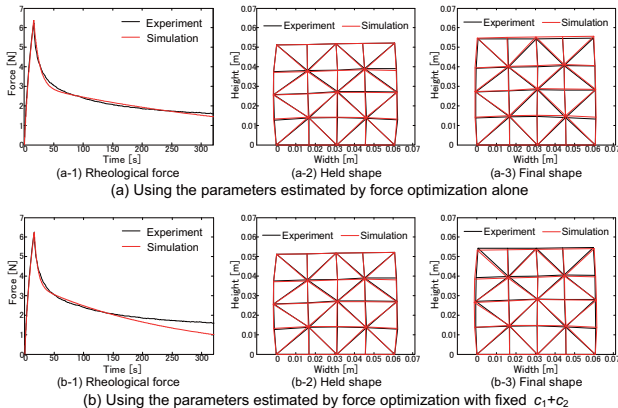


Fig. 7. Validation results of commercial available clay.

TABLE II
ESTIMATED PARAMETERS FOR SWEETS WITH NONLINEAR MODEL

Parameters	Estimated results	Parameters	Estimated results
E_1 (Pa)	1.0553×10^4	E_2 (Pa)	3.7340×10^4
c_1 (Pa·s)	6.6093×10^6	c_2 (Pa·s)	7.8618×10^4
α_1 (Pa·s)	6.6027×10^6	α_2 (Pa·s)	3.7403×10^4

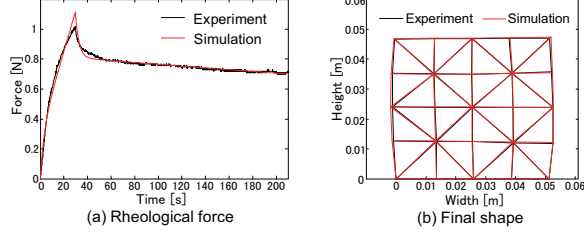


Fig. 9. Validation results of sweets material with the nonlinear model.

Eq. 29 with the following two equations:

$$\begin{aligned} \dot{\mathbf{F}}_1 &= -\frac{E_1}{\kappa\alpha_1 + c_1} \mathbf{F}_1 + (\lambda_1^{ela} \mathbf{J}_\lambda + \mu_1^{ela} \mathbf{J}_\mu) \mathbf{v}_N, \\ \dot{\mathbf{F}}_2 &= -\frac{E_2}{\kappa\alpha_2 + c_2} \mathbf{F}_2 + (\lambda_2^{ela} \mathbf{J}_\lambda + \mu_2^{ela} \mathbf{J}_\mu) \mathbf{v}_N. \end{aligned} \quad (37)$$

Using the parameter estimation methods proposed in the last section, we could determine all the parameters for Japanese sweets material based on the new model, as given in Table II. Simulation results compared with experimental measurements were shown in Fig. 9. We could now achieve good reproduction of both rheological force and residual deformation simultaneously.

VI. CONCLUSIONS AND FUTURE WORK

In this paper, we summarized physical models for simulating rheological objects. We formulated the generalized constitutive laws for both serial and parallel models. We found that serial and parallel models have the identical constitutive laws and they could be replaced by each other with small changes of some coefficients. We also found that the serial models are appropriate for calculating strain while the parallel models are convenient for calculating stress. Analytical expressions of rheological forces and residual deformation for generalized parallel models were derived. Theoretical discussions showed the difficulty for linear models to reproduce rheological forces and residual deformation simultaneously. A simpler 2D FE dynamic model and a more efficient method for parameter estimation were presented by taking the advantages of the analytical force expressions. Instead of iterative FE simulations, the parameter estimation method proposed in this paper only involved direct calculations of force expressions and we could obtain an optimal solution within only several seconds. To validate our modeling and parameter estimation methods, experiments with commercial clay and Japanese sweets materials were performed. We found that the value of $c_1 + c_2$ strongly affected both force amplitudes and the residual deformation. We failed to reproduce both force and recovered shape

simultaneously for sweets materials and we believe that the linear viscous elements caused the failure. Therefore, a dual-moduli viscous element was then introduced to improve our FE model and simultaneous reproduction of rheological force and deformation were finally achieved.

In the future, nonlinear modeling of rheological objects will be investigated except switching parameters. Biological organs and tissues, such as porcine livers and brain tissues, will be employed to validate our modeling and parameter estimation methods.

ACKNOWLEDGMENTS

This research is supported in part by Grant in Aid for Scientific Research (No. 20246049) and R-GIRO program of Ritsumeikan University.

REFERENCES

- [1] D. Terzopoulos, J. Platt, A. Barr, and K. Fleischer, "Elastically deformable models", *Proc. 14th Annual Conference on Computer Graphics and Interactive Techniques (SIGGRAPH '87)*, pp. 205–214, Anaheim, 1987.
- [2] D. Terzopoulos and K. Fleischer, "Modeling inelastic deformation: viscoelasticity, plasticity, fracture", *SIGGRAPH '88*, pp. 269–278, Atlanta, 1988.
- [3] M. Hrapko, J.A.W. van Dommelen, G.W.M. Peters, and J.S.H.M. Wismans, "The mechanical behaviour of brain tissue: Large strain response and constitutive modelling", *Biorheology*, vol. 43, pp. 623–636, 2006.
- [4] A. Nava, E. Mazza, M. Furrer, P. Villiger, and W.H. Reinhart, "In vivo mechanical characterization of human liver", *Med. Image Anal.*, vol. 12, pp. 203–216, 2008.
- [5] P.Y. Chua, T. Ilschner, and D.G. Caldwell, "Robotic manipulation of food products—a review", *Ind. Robot*, vol. 30, pp. 345–354, 2003.
- [6] H. Yoshida, Y. Murata, and H. Noborio, "A Smart Rheologic MSD Model Pushed/Calibrated/Evaluated by Experimental Impulses," *Proc. IEEE/RJS International Conference on Intelligent Robots and Systems (IROS '05)*, pp. 269–276, Edmonton, 2005.
- [7] T. Ikawa and H. Noborio, "On the Precision and Efficiency of Hierarchical Rheology MSD Model," *IROS '07*, pp. 376–383, San Diego, 2007.
- [8] B. A. Liloyd, G. Székely, and M. Harders, "Identification of spring parameters for deformable object simulation," *IEEE Trans. Vis. Comput. Graph.*, vol.13, no.5, pp. 1081–1094, Sept./Oct., 2007.
- [9] N. Sakamoto, M. Higashimori, T. Tsuji, and M. Kaneko, "An Optimum Design of Robotic Hand for Handling a Visco-elastic Object Based on Maxwell Model," *Proc. IEEE International Conference on Robotics and Automation (ICRA '07)*, pp. 1219–1225, Roma, 2007.
- [10] C.-H.D. Tsai, I. Kao, N. Sakamoto, M. Higashimori, and M. Kaneko, "Applying Viscoelastic Contact Modeling to Grasping Task: An Experimental Case Study," *IROS '08*, pp. 1790–1795, Nice, 2008.
- [11] Y.-H. Chai, G. R. Luecke, and J. C. Edwards, "Virtual Clay Modeling Using the ISU Exoskeleton," *Proc. IEEE Virtual Reality Annual International Symposium (VRAIS '98)*, pp. 76–80, Atlanta, 1998.
- [12] E. Samur, M. Sedef, C. Basdogan, L. Avtan, and O. Duzgun, "A robotic indenter for minimally invasive measurement and characterization of soft tissue response," *Med. Image Anal.*, vol.11, pp. 361–373, Aug., 2007.
- [13] B. Ahn and J. Kim, "Measurement and characterization of soft tissue behavior with surface deformation and force response under large deformations," *Med. Image Anal.*, vol.14, pp. 138–148, 2010.
- [14] J. Muramatsu, T. Ikuta, S. Hirai, and S. Morikawa, "Validation of FE deformation models using ultrasonic and MR images," in *Proc. 9th International Conference on Control, Automation, Robotics and Vision (ICARCV'06)*, pp. 1–6, Singapore, 2006.
- [15] Z. Wang, K. Namima, and S. Hirai, "Physical parameter identification of rheological object based on measurement of deformation and force," *ICRA '09*, pp. 1238–1243, Kobe, 2009.
- [16] Z. Wang and S. Hirai, "Modeling and parameter identification of rheological object based on FE method and nonlinear optimization," *IROS '09*, pp. 1968–1973, St. Louis, 2009.